# CHAPTER 6 THREE-DIMENSIONAL ANALYSIS -- NUMERICAL MODEL C

## 6.1 INTRODUCTION

This chapter describes the analysis using numerical model C, a symmetric three-pipe system (defined in Section 6.2). From the study of the results from numerical models A and B in Chapters 4 and 5, it is known that the non-uniform distribution of the load at the pipe joint induces not only concentrated compressive stresses, but also high tensile stresses in the concrete pipe. In fact, once the load distribution on the pipe ends is known, it is easy to obtain the stresses within the concrete pipe by using the numerical model B described in Chapter 5 and the results can then be used to estimate the safety of the jacking pipe in practice. To obtain load distributions at the pipe joint with a misalignment of the pipeline during pipe jacking, the analyses were carried out with numerical model C and the results from this model are examined in this chapter. To extend the two-dimensional work and to verify the conclusions from the two-dimensional model, similar aspects were investigated using the numerical model C under full three-dimensional conditions.

Again, the concrete pipe, the surrounding soil and the packing material are all treated as linearly elastic throughout this chapter. The material constants for the concrete pipe and the soil are the same as those used in Chapter 5, that is, a Young's modulus $E_c$ = 40000MPa and a Poisson's ratio $\mu_c$ = 0.2 for the concrete pipe, and a Young's modulus $E_s$ = 144MPa and a Poisson's ratio $\mu_s$ = 0.2 for the soil. Similar material constants of packing material used in Chapter 3 are adopted here to study the influence of the properties of the packing material.

In this chapter, the numerical model C is described in Section 6.2. The effect of the properties of the packing material and the effect of the pipeline misalignment are discussed in Sections 6.3 and 6.4 respectively. Finally, the conclusion is given in Section 6.5.

## 6.2 NUMERICAL MODEL C

One common misalignment of the pipeline is caused by gradual changes in direction of the pipeline as shown in Figure 6.1. For simplicity, it is assumed that the jacking force on the left end and the reaction force on the right end are symmetrical about the plane z = 0 and that the misalignment angles $\beta_1$ and $\beta_2$ have the same value. So it is simplified as a symmetrical problem about the plane z = 0 ( it should be pointed out here that similar symmetries have been applied in the numerical model A and B for the 'edge' loading condition in Chapters 4 and 5). To model this simplified problem, numerical model C is established as shown in Figure 6.2. The model consists of a half pipe with its surrounding soil at the bottom, a complete pipe on the top and a packing material between the two pipes. The soil is included to avoid any local effect of constraints as discussed in Chapter 4. The dimensions of the model are also shown in the figure. For numerical convenience, there was just one interface used between the packing material and the bottom pipe in analysis. Furthermore, the geometry of the domain and the loads are also symmetric about the plane y = 0, so just a quarter of the problem was used in the analysis.

The three-dimensional finite element mesh of the numerical model C used in the analysis is shown in Figure 6.3(a); the unfolded surface of r = 600mm is in Figure 6.3(b); the section of z = 0mm is in Figure 6.3(c) and the section of $\theta = 0^0$ is in Figure 6.3(d). For the boundary conditions in the numerical analysis, the nodes on the outer surface of the soil mesh were all fixed in both $x$ and $y$ directions, while the nodes on the plane z = 0 were fixed in the $z$ direction and the nodes on the plane $y = 0$ were fixed in the $y$ direction due to the symmetrical condition. The main element type used in the analysis was the 8-node hexahedron, while quadrilateral interface elements were used between the packing material and the bottom pipe. In the analysis, the misalignment angle $\beta$ of the pipe line was simulated by giving an equivalent displacement $\delta$ in $x$ direction at the upper end of the top pipe as shown in Figure 6.2. Equivalence means that if the displacement at the centre of the bottom end of the top

pipe is zero, the displacement $\delta$ in the $x$ direction at the upper end will produce the same rotation angle $\beta$ (that is, $\tan\beta = \delta / L$, where $L$ is the pipe length). The applied jacking force was assumed uniformly distributed over the upper pipe end with a load intensity q = 10MPa as shown in Figure 6.2. For numerical convenience, the analysis was carried out in two stages. At first, 20% of the total load was applied without rotation of the top pipe, then the other 80% of the total load and the rotation of the top pipe were applied simultaneously. The stresses in the contours of this chapter are all normalized with respect to q = 10MPa.

Similar to the analysis described in Chapter 3, the interaction between the bottom pipe and the packing material was modelled by an elastic perfectly-frictional Mohr-Coulomb model described in Chapter 2 with the normal stiffness $K_n$ = 800MPa /mm, the shear stiffness $K_s$ = 400MPa/mm, the frictional angle $\phi = 20^0$, the dilation angle $\psi = 20^0$ and the cohesion parameter c = 0.05MPa.

## 6.3 EFFECT OF THE PROPERTIES OF THE PACKING MATERIAL

In this section, the effect of the properties of the packing material, the shear modulus and the Poisson's ratio of the packing material, is investigated. In the analysis, the packing material was linearly elastic with two different shear moduli $G_p$ = 300MPa and 900MPa simulating soft and stiff packing materials, and with different Poisson's ratios $\mu_p$ = 0.1, 0.4 and -0.3 representing low, high and negative Poisson's ratio respectively as in Chapter 3. The applied displacement in the $x$ direction at the upper end of the top pipe was $\delta$ = 3.93mm which is equivalent to a rotation angle $\beta = 0.09^0$ of the top pipe.

The solution procedure used in the analysis was the initial stiffness method described in Chapter 2. There was just one step in the first calculation stage with 20% applied load since the interface was elastic. In the second calculation stage there are 250 and 300 steps in the

case $G_p$ = 300MPa and 900MPa respectively and there were several iterations within each step depending on solution convergence.

### 6.3.1 EFFECT OF THE POISSON'S RATIO

The analysis of the effect of the Poisson's ratio of the packing material was carried out with the shear modulus $G_p$ = 300MPa corresponding to a soft packing material and three different Poisson's ratios $\mu_p$ = 0.1, 0.4 and -0.3.

The normalized normal stresses on the interface are shown in Figures 6.4(a), 6.4(b) and 6.4(c) for the case of $\mu_p$ = 0.1, 0.4 and -0.3 respectively. From the figure, it is clear that in the case of $\mu_p$ = 0.1 and $\mu_p$ = -0.3 the stress distribution patterns are very similar showing an almost linear distribution with $x$. In the case of $\mu_p$ = 0.4, the normal stresses have a similar linear distribution when $\theta > 120^0$, while in the region $\theta < 120^0$ the stresses have lower magnitudes at the two sides r=600mm and r=715mm and a higher magnitude at the middle on the line x = constant. In general, the stresses are zero ( or almost zero ) in the region of $x$ = -715mm, and the stress magnitudes increase with $x$ and reach their peak values at $x$ = 715mm. (Note: The higher stress magnitude in the case of $\mu_p$ = 0.4 is possibly due to the higher stiffness of the packing material since $E_p = 2\ G_p\ (\ 1 + \mu_p\ )$, however, the different distribution pattern in the case of $\mu_p$ = 0.4 is mainly due to the high Poisson's ratio because the distribution patterns are similar in the case of $\mu_p$ = 0.1 and $\mu_p$ = -0.3 without the influence of the stiffness of the packing material.)

The normalized shear stresses on the interface are shown in Figure 6.5(a), 6.5(b) and 6.5(c) for the cases $\mu_p$ = 0.1, 0.4 and -0.3 respectively. The figure shows that the distribution patterns of the shear stresses are more complicated than those of the normal stresses. In the case of $\mu_p$ = 0.1, the stresses increase when $\theta$ decreases in the region of

$\theta > 110^0$ ; and in the region of $\theta < 70^0$ , the stresses increase with $\theta$ on the line r = constant and increase with r on the line $\theta$ = constant. The high stresses are located in the region of $\theta = 90^0$ . In the case with negative Poisson's ratio ( $\mu_p$ = -0.3), the stresses have a similar distribution pattern as that in the case of $\mu_p$ = 0.1 except in the region of $\theta < 70^0$ where the stresses reduce when r increases on the line $\theta$ = constant. In the case of $\mu_p$ = 0.4, the stresses almost increase linearly with $x$ in the region of $0 > 110^0$ ; and in the region of $\theta < 110^0$ , the stresses are higher on the two sides especially on the outer side ( r = 715mm ). The peak stresses are similar in the case of $\mu_p$ = 0.1 and -0.3, and much higher in the case of $\mu_p$ = 0.4. (Note: With $E_p = 2\ G_p ( 1 + \mu_p )$, the difference of the stiffness between the case of $\mu_p$ = -0.3 and $\mu_p$ = 0.1 is larger than that between the case of $\mu_p$ = 0.4 and $\mu_p$ = 0.1. However, the shear stresses in the case of $\mu_p$ = -0.3 and $\mu_p$ = 0.1 are similar and quite different from those in the case of $\mu_p$ = 0.4. This means that the difference is due to the influence of the high Poisson's ratio of the packing material.)

After the discussion about the stresses on the interface, the stresses within the concrete pipes are examined. In order to avoid the average effect of the stresses from packing materials and the interface and to obtain a better view of the stress contours, the packing material and the interface are removed in the stress contours of the concrete pipes throughout this chapter.

The normalized most tensile principal stresses in the concrete pipes are shown in Figure 6.6(a), 6.6(b) and 6.6(c) for the cases of $\mu_p$ = 0.1, 0.4 and -0.3 respectively. The figure shows that in all three cases the stress distribution patterns are similar to some extent. The high tensile stresses are mainly within the top pipe at the top right and bottom left corners and in the region of $\theta = 90^0$ on the upper end except in the case $\mu_p$ = 0.4 where the high tensile stresses also exist at the joints of both pipes in the region $\theta = 0^0$ . The peak values are similar in all three cases with the highest stress in the case of $\mu_p$ = 0.4. The tensile stresses in these high stress regions are mainly in the hoop direction in all three cases as shown in

Figure 6.6(d). ( The tensile stresses on the upper end of the top pipe are due to the given displacements on that end, which are used to produce the misalignment needed to examine the behaviour of the pipe joint and the bottom pipe and might deviate from the loading and constraint conditions on this pipe end in practice. However, the effort in this Chapter is placed on the pipe joint and the bottom pipe.)

The normalized most compressive stresses in the pipes are shown in Figure 6.7. It is clear from the figure that the stress distributions are similar in all three cases. In the bottom pipe, the stresses are almost zero in the region of $\theta = 180^0$ and the stress magnitudes increase when $\theta$ decreases with its peak magnitude at $\theta = 0^0$. In the top pipe, the stresses are almost constant at the upper end with the magnitude of the applied load, while in the region of the pipe joint the stresses have similar patterns as those in the bottom pipe.

### 6.3.2 EFFECT OF THE SHEAR MODULUS

In this section, the effect of another property of the packing material, the shear modulus, is examined. Since a low shear modulus was used in the analysis of the effect of the Poisson's ratio of the packing material, a high shear modulus ($G_p$ = 900MPa) was used in the analysis described in this section with the same three different Poisson's ratios $\mu_p$ = 0.1, 0.4 and -0.3. The results are compared with those in Section 6.3.1.

Again, the normalized stresses on the interface are discussed first. The normalized normal stresses in case $\mu_p$ = 0.1, 0.4 and -0.3 are now shown in Figure 6.8(a), 6.8(b) and 6.8(c) respectively. The figure shows that the stress patterns are very similar to those with the low shear modulus $G_p$ = 300MPa except that the areas with zero stresses in the region $\theta = 180^0$ are larger than those with $G_p$ = 300MPa and that the peak values are higher than

those with $G_p$ = 300MPa. The peak magnitudes of stress in all three cases are similar with the highest magnitude still in the case of $\mu_p$ = 0.4.

The normalized shear stresses on the interface are given in Figure 6.9(a), 6.9(b) and 6.9(c) for the case $\mu_p$ = 0.1, 0.4 and -0.3. Again, the stresses in all three cases show similar distribution patterns to those with $G_p$ = 300MPa except that the peak stresses increase in the case of $\mu_p$ = 0.1 and -0.3 and reduce in the case of $\mu_p$ = 0.4. However, the highest shear stress is still in the case of $\mu_p$ = 0.4. ( Following the same argument in Section 6.3.1 for Figure 6.5, it is known that difference of the shear stresses on the interface is mainly due to the influence of the Poisson's ratio. The comparison of the results in Figures 6.5 and 6.9 suggests that the influence of the Poisson's ratio reduces when the shear modulus increases.)

Figure 6.10 shows the normalized most tensile principal stresses in the concrete pipes. Clearly, the stress distribution patterns are very similar to those with the low shear modulus as shown in Figure 6.6. The direction of the tensile stresses in all three cases is also mainly in the hoop direction as with $G_p$ = 300MPa (refer to Section 6.3.1 and see Figure 6.6(d)). For the most compressive stresses in the pipes, the distribution patterns are very similar to those with $G_p$ = 300MPa except that the peak magnitudes are just slightly higher (the stress contours are not included here to avoid repetition, refer to Section 6.3.1 and see Figure 6.7).

## 6.4 EFFECT OF THE PIPELINE MISALIGNMENT

In Section 6.3, the effect of the properties of the packing material have been studied. The effect of the misalignment of the pipe line is examined in this section. Again, in the analysis the soil and the packing material were treated as linearly elastic with the same material constants as in the Section 6.3. The applied misalignment angle of the pipe line was $\beta = 0.27^0$ which was simulated in the analysis by the equivalent given displacement of

$\delta$ = 11.78mm in the $x$ direction at the upper end of the top pipe. The load, boundary conditions and the properties of the interface were unchanged.

The solution procedure used in this section is also the initial stiffness method described in Chapter 2. There was again one step in the first stage with 20% applied load. In the second calculating stage, the other 80% load and the rotation of $\beta = 0.27^0$ of the top pipe were applied and there were 400 and 500 steps in the case $G_p$ = 300MPa and 900MPa respectively with several iterations within each step depending on convergence and controlled by the program.

### 6.4.1 ANALYSIS WITH SOFT PACKING MATERIAL

At first, the analysis was carried out with a soft packing material ($G_p$ = 300MPa) and with the same three Poisson's ratios $\mu_p$ = 0.1, 0.4 and -0.3. The normalized normal stresses on the interface are given in Figure 6.11(a), 6.11(b) and 6.11(c). From the figure, it is clearly seen that the stress patterns are similar in all three cases. The stresses are zero in the region of $\theta > 100^0$ (the exact regions are slightly different in different cases as shown in the figure) and in general the stresses increase when $\theta$ reduces in the region of $\theta < 100^0$. The changes of the stresses across the thickness of the pipe are significant especially in the case of $\mu_p$ = 0.4. The maximum values of the stress magnitudes are similar in all three cases but are much higher than those in Section 6.3.1 with $\beta = 0.09^0$ and the highest magnitude is in the case of $\mu_p$ = 0.4.

Figure 6.12 shows the normalized shear stresses on the interface. Again, in all three cases there is a large area with zero stress in the region about $\theta > 100^0$ on the interface. This means that there is a big gap between the packing material and the bottom pipe in all three cases with this misalignment angle $\beta = 0.27^0$. High stresses in all three cases are located on

the outer side of the cross section (r=715mm) with its centre in the region of $\theta$=54$^0$, 48$^0$ and 58$^0$ in the case of $\mu_p$ = 0.1, 0.4 and -0.3 respectively. In general, the stresses reduce when away from the high stress centre except in the case of $\mu_p$ = 0.4 where the high stresses also exist at the outer side of the cross section over all of the region of $\theta < 65^0$. The peak values of the stress are much higher than those with $\beta = 0.09^0$ in Section 6.3.1 and the highest stress is also in the case of $\mu_p$ = 0.4.

The normalized most tensile stresses within the concrete pipes are shown in Figure 6.13(a), 6.13(b) and 6.13(c) for the three cases $\mu_p$ = 0.1, 0.4 and -0.3. The stress patterns are similar in all three cases but quite different from those in Section 6.3.1 with $\beta = 0.09^0$ due to the big gap on the interface. The high stresses are now at the pipe joint of the bottom pipe with its centre in the region of $\theta = 90^0$ (in fact, the stress patterns in the bottom pipe are similar to those in Figure 5.3 in Chapter 5 since the bottom pipe is also under 'edge' loading condition). The stresses in other domains are small. The peak values of the stress are similar in all three cases but much higher than those with $\beta = 0.09^0$ in Section 6.3.1. The highest stress is still in the case of $\mu_p$ = 0.4. The tensile stresses in the high stress region are mainly in the hoop direction in all three cases as shown in Figure 6.13(d).

Figure 6.14 gives the distributions of the normalized most compressive principal stresses within the concrete pipes. The stress patterns are similar in all three cases to some extent. In the bottom pipe, the stresses are almost zero in the region of $\theta > 90^0$ and the magnitude of the stress increases when $\theta$ reduces in the region of $\theta < 90^0$ with the peak magnitudes in the region of $\theta < 10^0$. In the top pipe, the stresses are almost constant at the upper end of the pipe with the magnitude of the applied load. In general, the stress magnitudes increase when $\theta$ reduces on a section z = constant. The peak stress magnitudes are similar in all three cases and are much higher that those with $\beta = 0.09^0$ as shown in Figure 6.7.

### 6.4.2 ANALYSIS WITH STIFF PACKING MATERIAL

This section describes the analysis with a stiff packing material ($G_p$ = 900MPa) and with all other conditions unchanged as in Section 6.4.1. The normalized normal stresses on the interface are now shown in Figure 6.15. When comparing with Figure 6.11 in Section 6.4.1, it can be seen that the stress distributions on the interface are very similar apart from three small differences. The first difference is that the areas with zero stresses are slightly larger than with the soft packing material. The second difference is that the changes of the stresses across the pipe thickness are more significant than with the soft packing material. Finally, the peak stress values are higher and the difference of the peak stresses between different cases with different Poisson's ratio reduces.

Figure 6.16 shows the normalized shear stresses on the interface. To some extent, the stress patterns are similar to those with soft packing as shown in Figure 6.12. The areas with zero stresses are larger than with soft packing as discussed for the normal stresses. This means that the gaps between the packing material and the bottom pipe are wider. Now the high stresses in all three cases are located in the same region of $\theta = 46^0$ and the peak values are higher than with soft packing, especially in the case $\mu_p$ = 0.1 and -0.3.

The normalized most tensile principal stresses within the concrete pipes are shown in Figure 6.17. From the figure, it is clear that the stress distribution patterns are similar to those with soft packing material as shown in Figure 6.13 except that the maximum values are higher than those with the soft packing material, especially in the case of $\mu_p$ = 0.1 and -0.3. The tensile stresses in the high stress regions are also in the hoop direction as with the soft packer (see Figure 6.13(d)). As for the most compressive principal stresses in the concrete pipes, the stress patterns and the peak stress magnitudes in all three cases are almost same as those with the soft packing material and are not discussed here in detail (refer to Section 6.4.1 and see Figure 6.14).

## 6.5 CONCLUSION

The numerical results from the analysis with numerical model C show that the misalignment of the pipeline induces not only high normal stresses but also high shear stresses at the pipe joint which in turn produce high concentrated compressive stresses and high tensile stresses in the jacking concrete pipes. The results from the analysis have given a good understanding about the effect of the misalignment of the pipeline and of the properties of the packing material. The two-dimensional analysis described in Chapter 3 has also shown a similar effect of the properties of the packing material and the effect of the misalignment. However, the three-dimensional results in this chapter give a clearer picture and better understanding about these aspects and also provide some new aspects which the two-dimensional model cannot take into account, for example, the distribution of the shear stresses at the pipe joint.

In general, the normal stresses on the interface increase with $x$ since the misalignment rotation is about the $y$ axis. However, the shear stress patterns on the interface are very complicated and the high stress centre is usually located on the outer side of the pipe thickness at the mid-way between the edge of the open gap and the right end ($\theta = 0^0$). The results also show that the high stresses are mainly at the pipe joint of the bottom pipe with the high applied misalignment angle. The stress distribution patterns in the bottom pipe are very similar to those in Chapter 5 under the 'edge' loading condition since the bottom pipe is assumed to be under a symmetrical loading condition, and this confirms that once the stresses at the pipe joint are known the numerical model B in Chapter 5 can be used to calculate the stresses in the concrete pipe.

From the results of numerical model C in this chapter, a few conclusions are drawn out as following:

(1) The dominating factor inducing high concentrated stresses in the concrete pipes is the misalignment angle of the pipeline, especially with the high rotation angle where the stress concentrations are enhanced due to the separation between the packing material and the concrete pipe. So the good control of this misalignment angle is critical in the practice of pipe jacking.

(2) Under the same condition, the packing material with high Poisson's ratio induces higher shear stresses on the interface and higher tensile stresses in the concrete pipe than that with low Poisson's ratio, while the material with a negative Poisson's ratio produces even better results although the difference between the low Poisson's ratio and the negative one is not significant. A negative Poisson's ratio is difficult to achieve, thus a good packing material should possess a very low Poisson's ratio. In practice, currently used packing materials, eg. chipboard and fibreboard have a Poisson's ratio close to zero.

(3) The high shear modulus also increases the stresses on the interface and in the pipe although not by a significant amount. This means that a good packing material should have a low shear modulus.

(4) In numerical model C, it means no packing material if the material constants of the packing material are same as those of the concrete pipe. Combining conclusion 2 and 3 above, it is clear that a good packing material will reduce the stresses in the concrete pipes.

(5) In the numerical model C, the bottom pipe is assumed under a symmetrical loading condition (or under an 'edge' loading condition). For more general loading conditions, a more complicated three-pipe model is needed in future research.

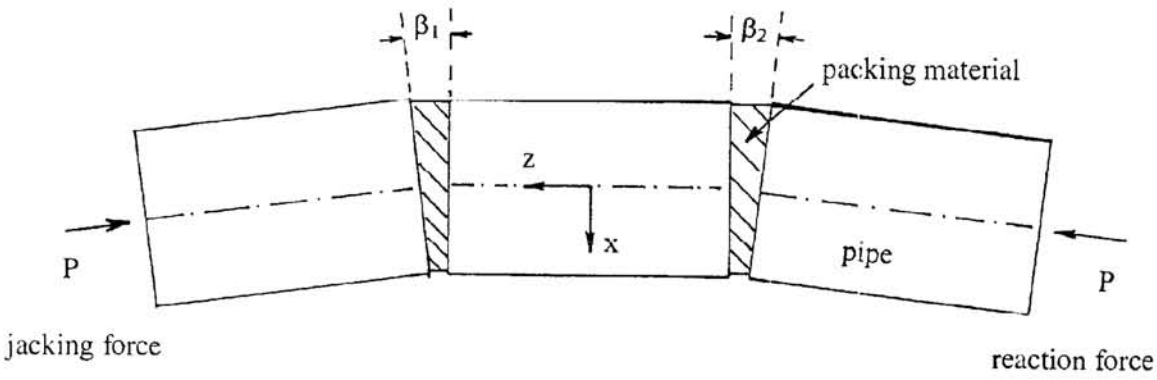


Figure 6.1 A common pipe line misalignment

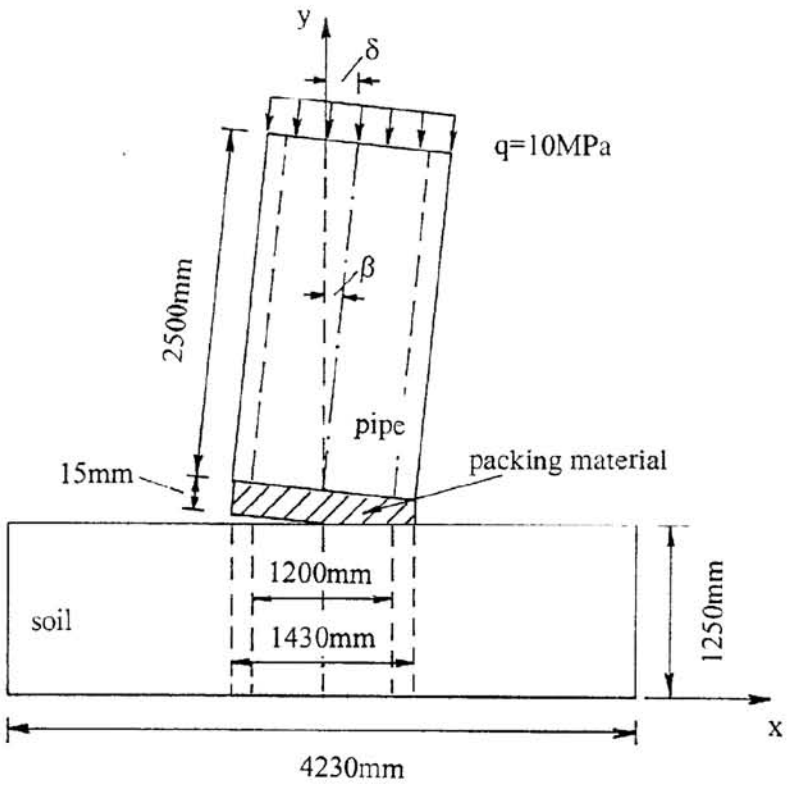


Figure 6.2 Numerical model C

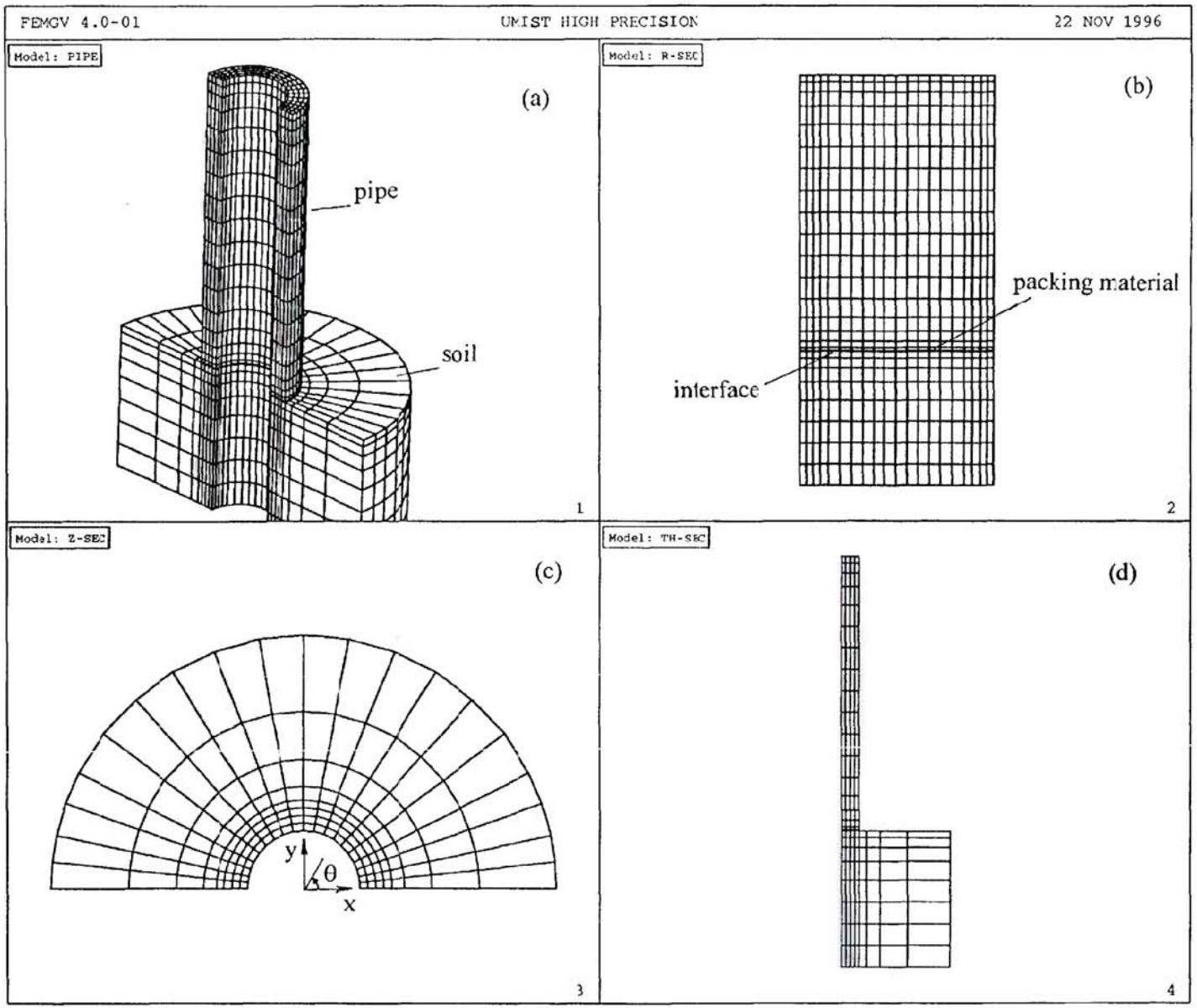


Figure 6.3 FE mesh of numerical model C

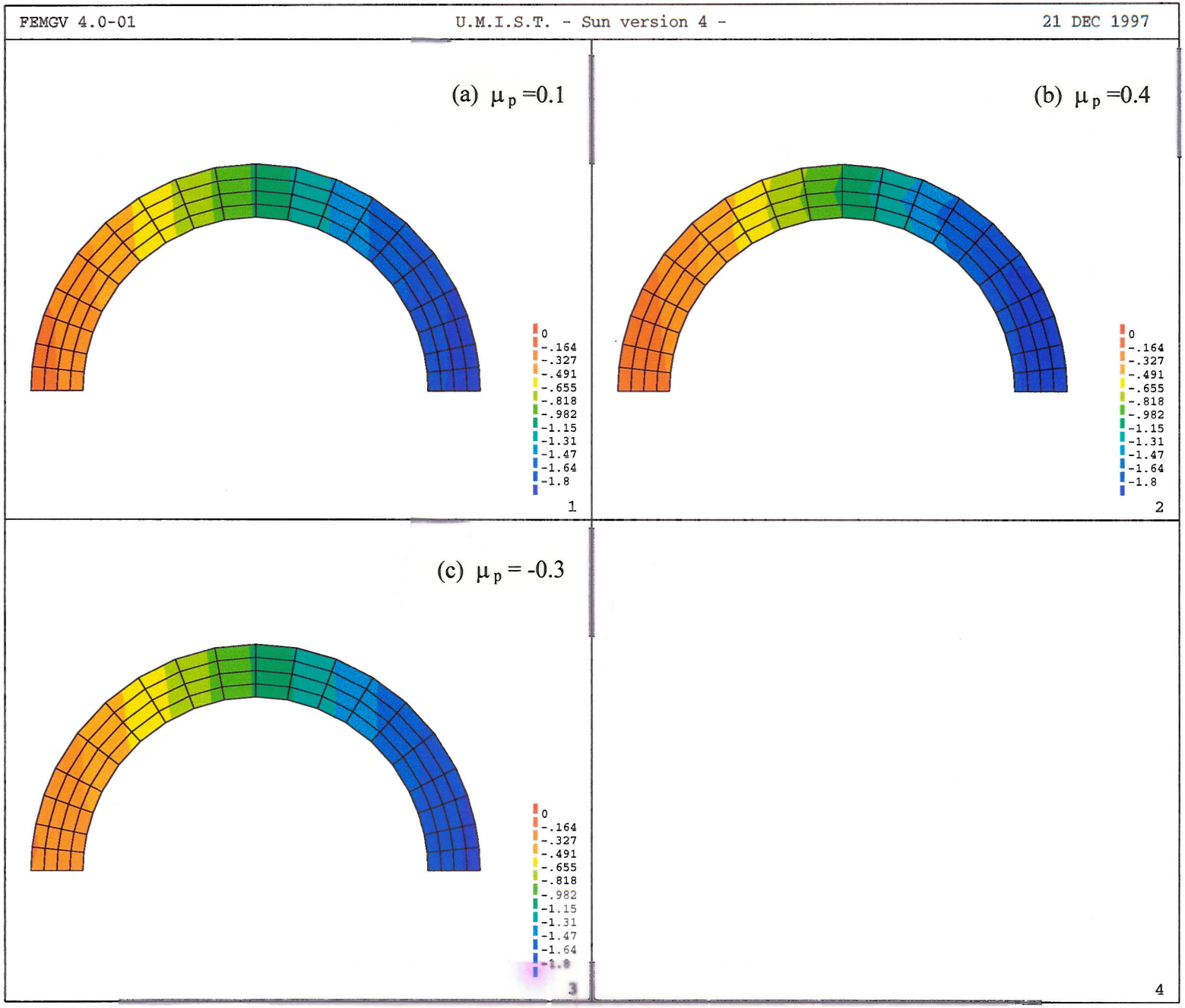


Figure 6.4 Normalized normal stresses on the interface with soft packing and $\beta=0.09^0$

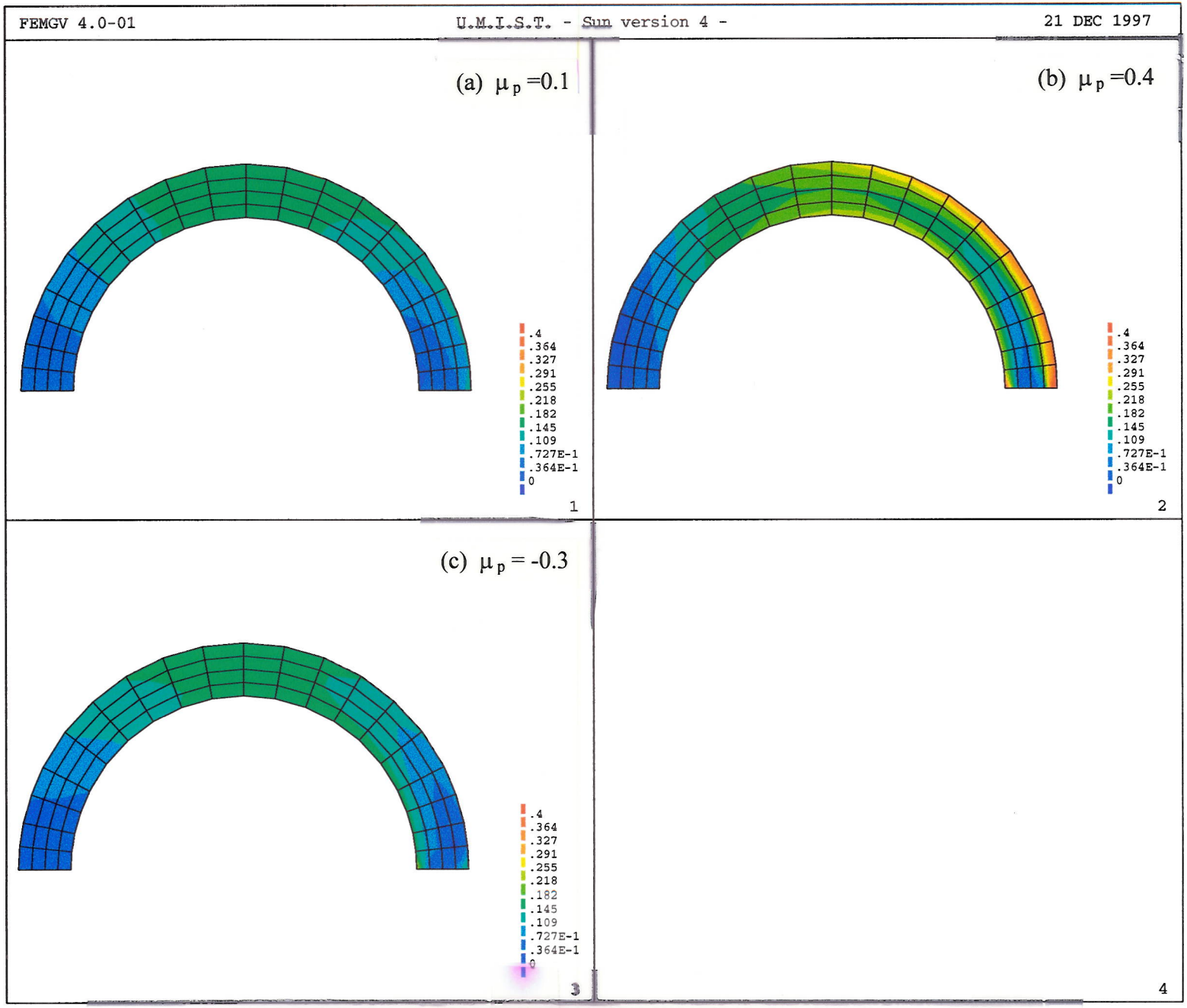


Figure 6.5 Normalized shear stresses on the interface with soft packing and $\beta=0.09^0$

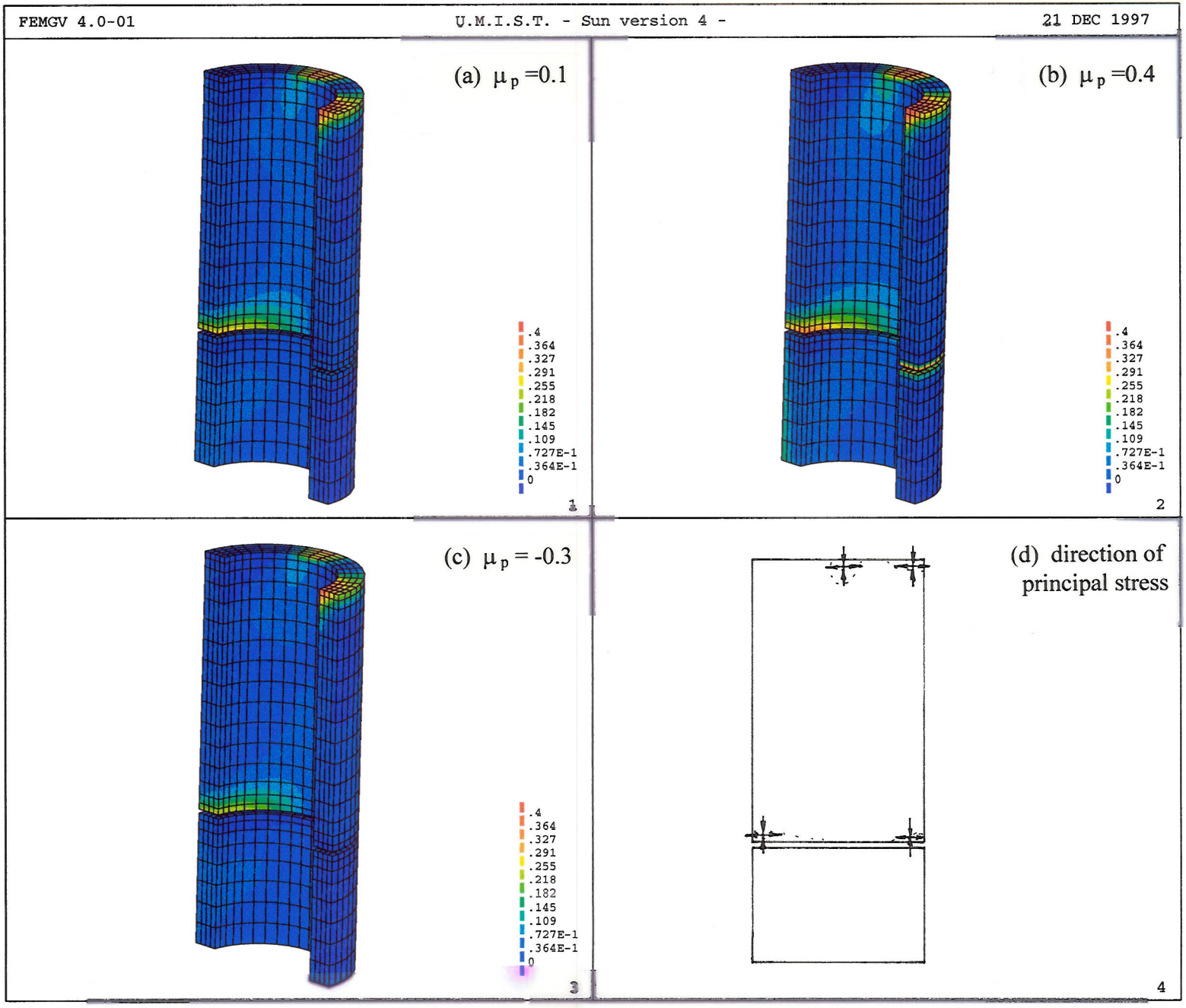


Figure 6.6 Normalized most tensile principal stresses in the pipes with soft packing and $\beta=0.09^0$

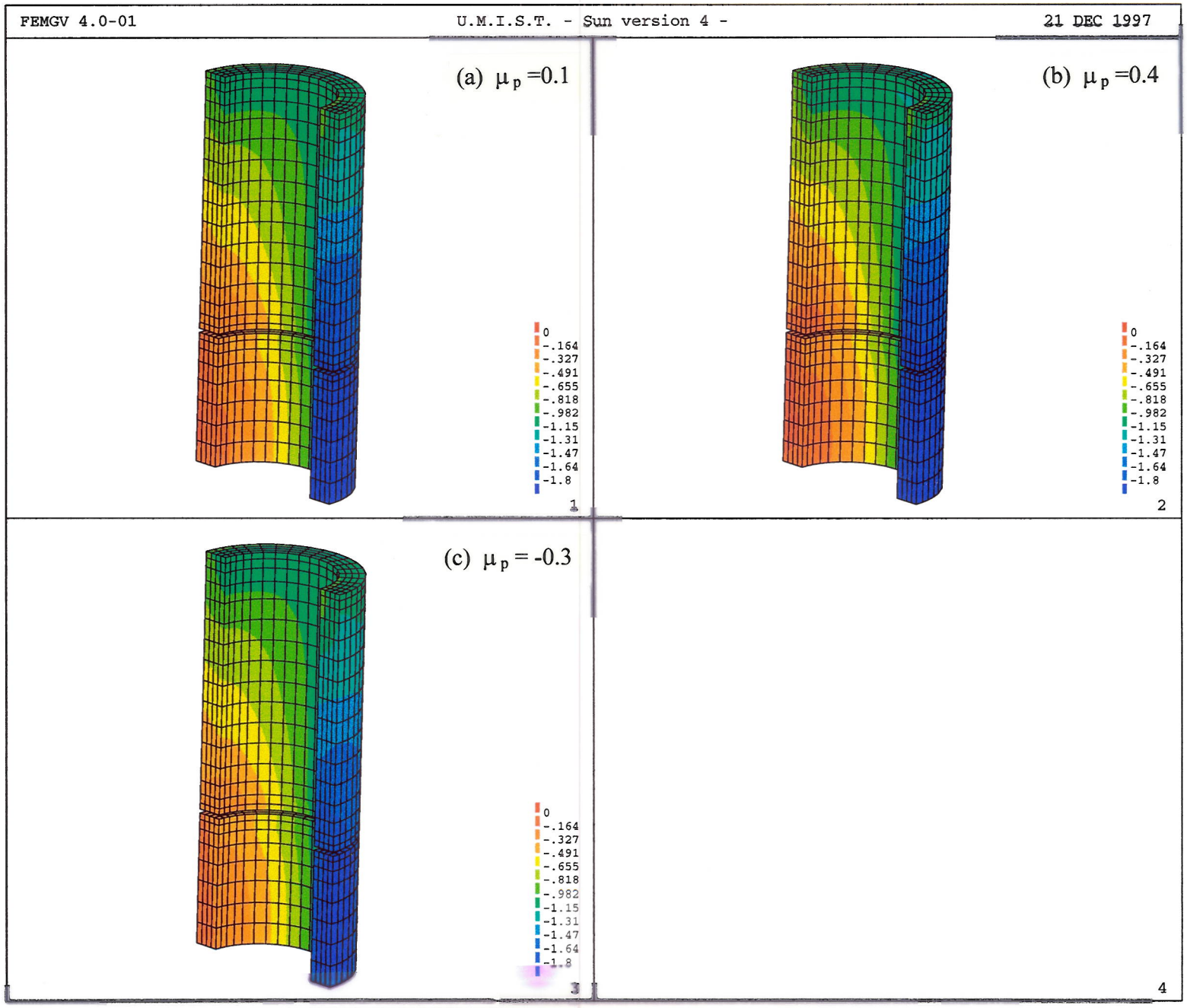


Figure 6.7 Normalized most compressive principal stresses in the pipes with soft packing and $\beta=0.09^0$

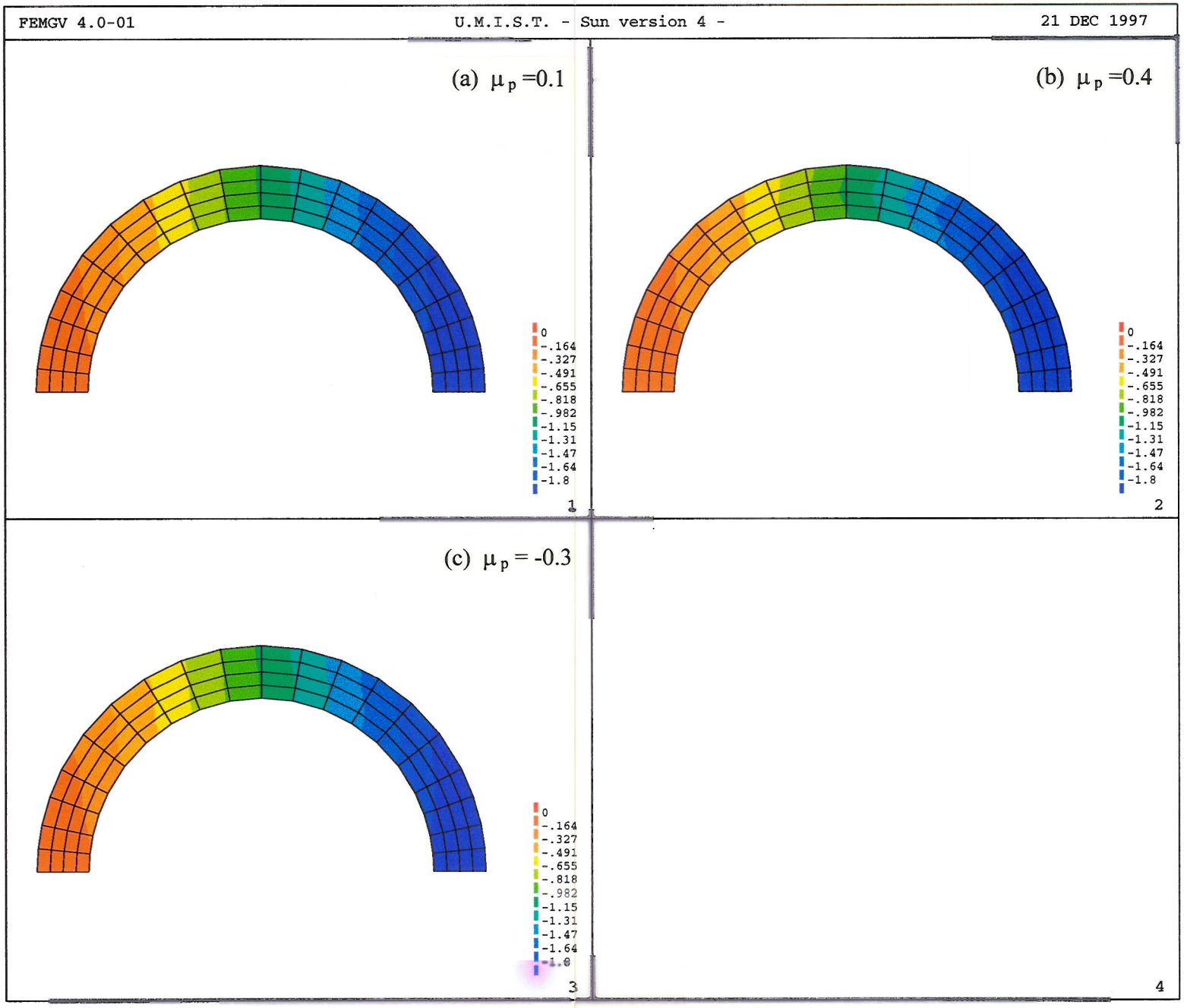


Figure 6.8 Normalized normal stresses on the interface with stiff packing and $\beta=0.09^0$

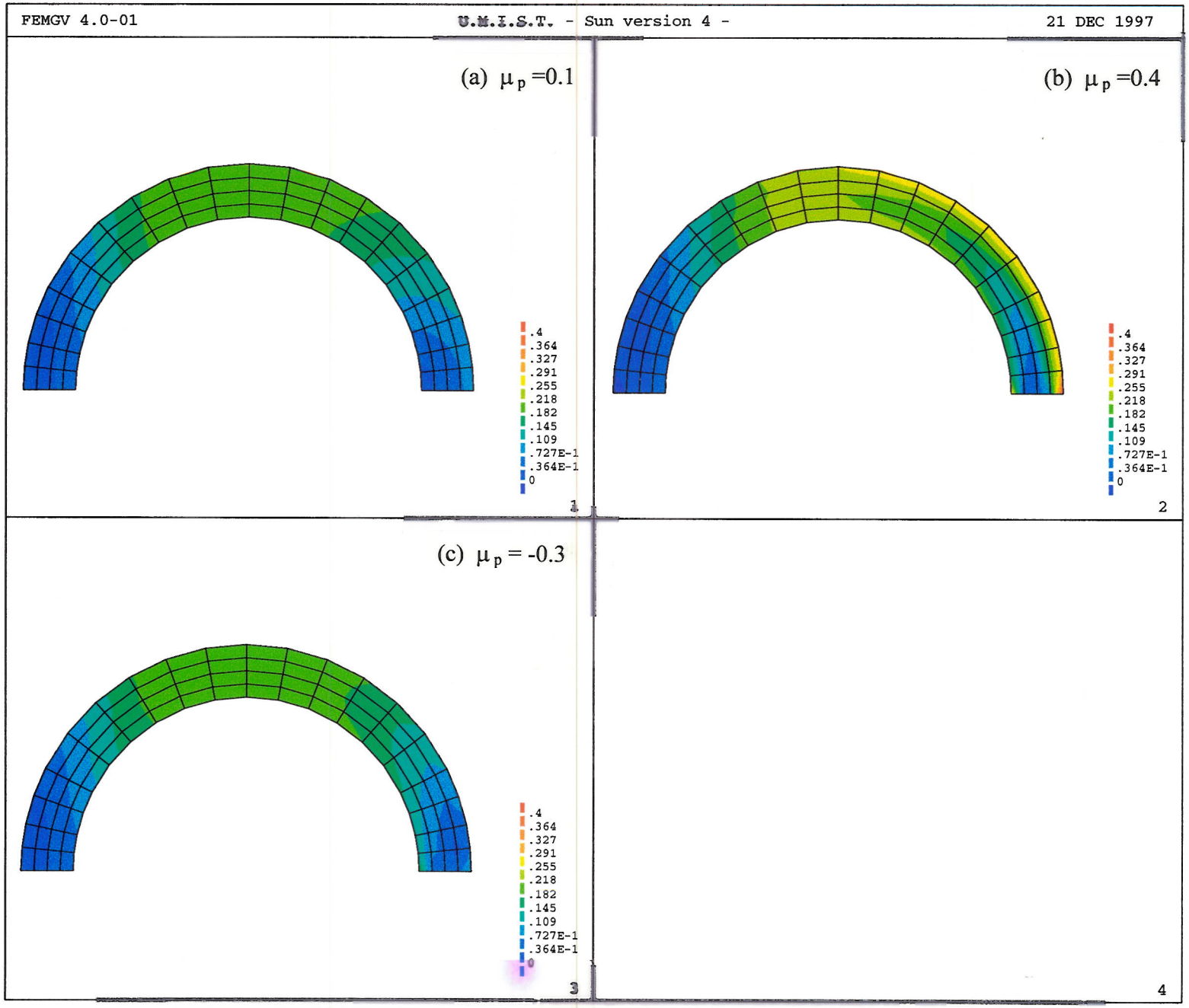


Figure 6.9 Normalized shear stresses on the interface with stiff packing and $\beta=0.09^0$

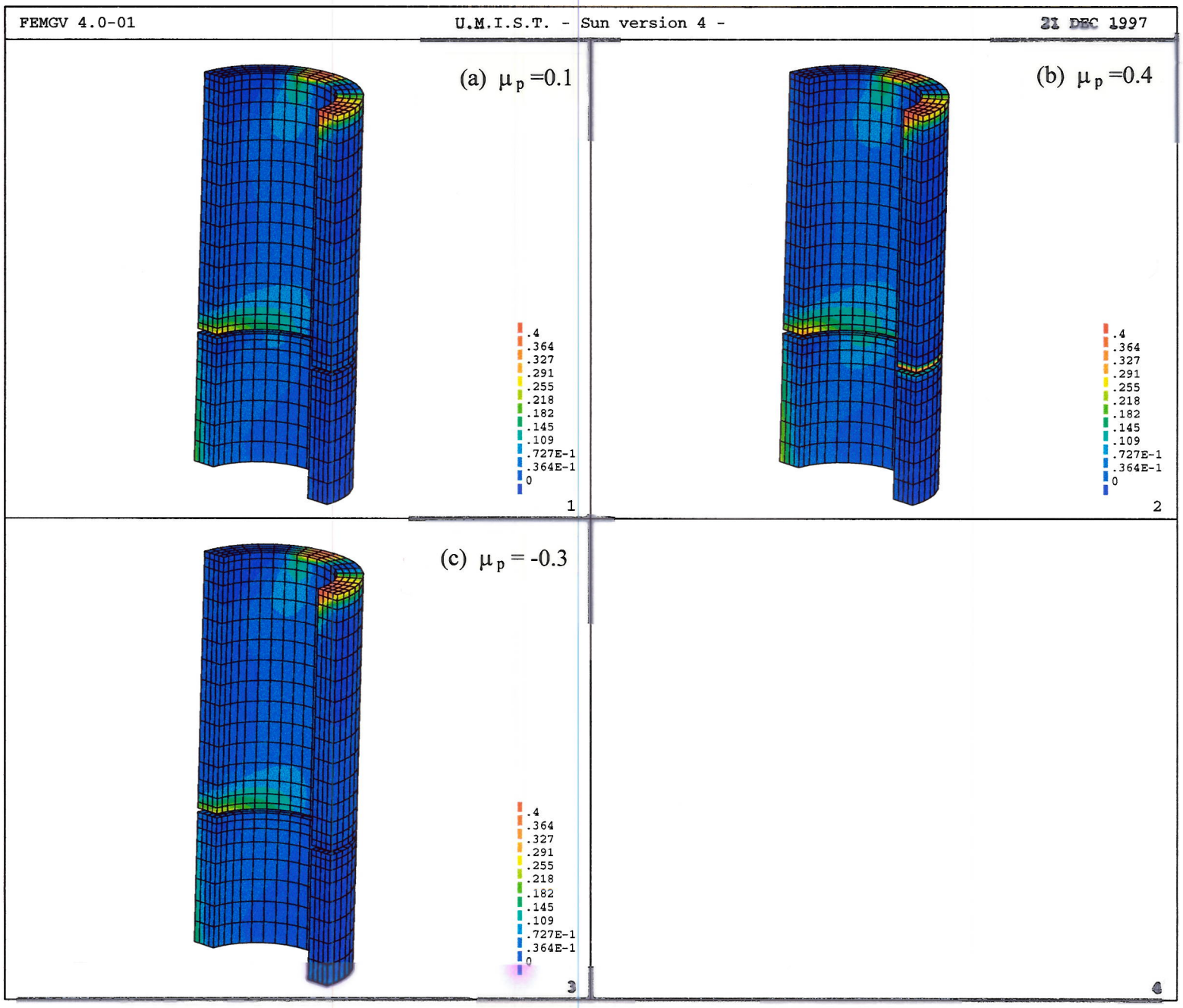


Figure 6.10 Normalized most tensile principal stresses in the pipes with stiff packing and $\beta=0.09^0$

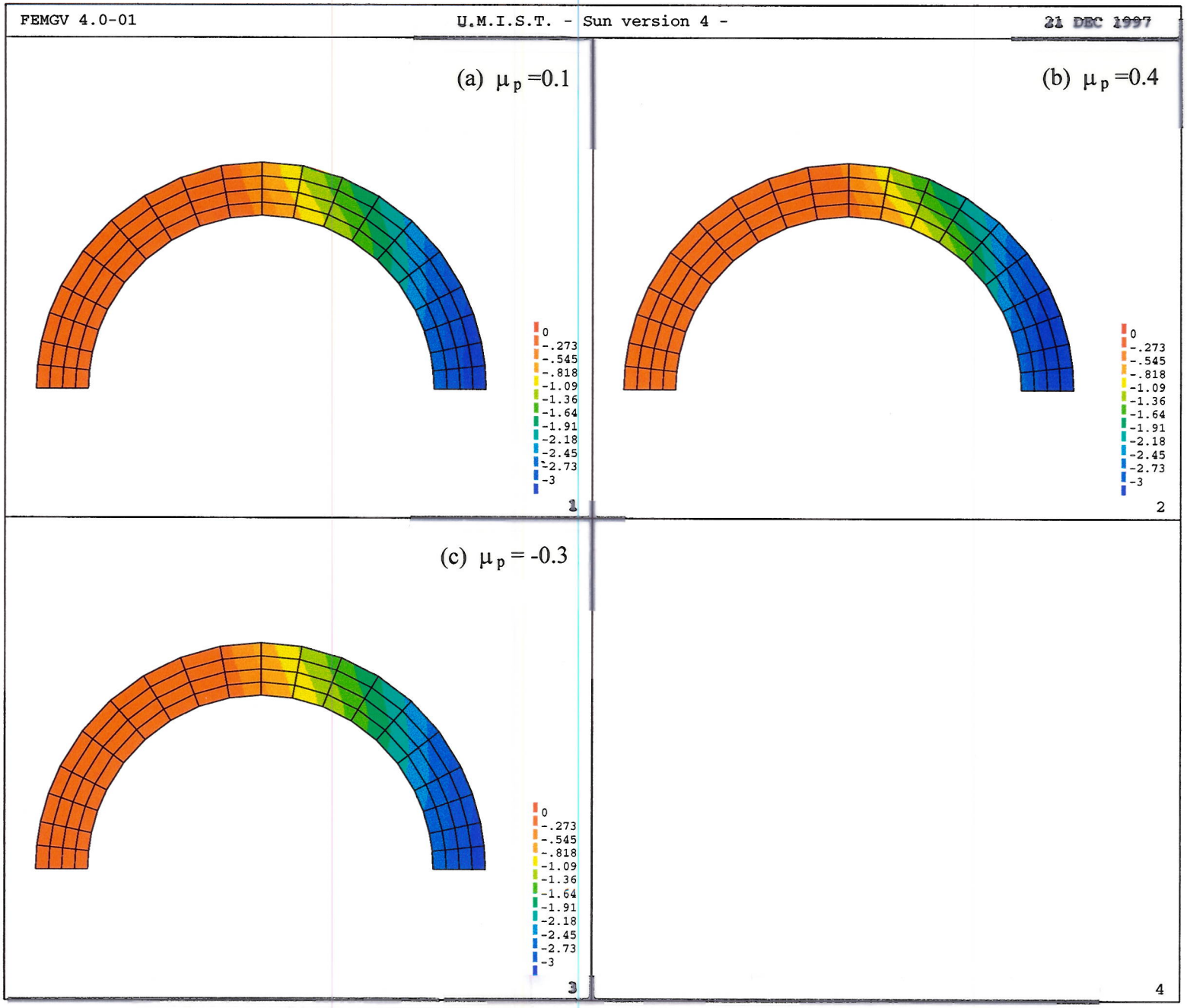


Figure 6.11 Normalized normal stresses on the interface with soft packing and $\beta=0.27^0$

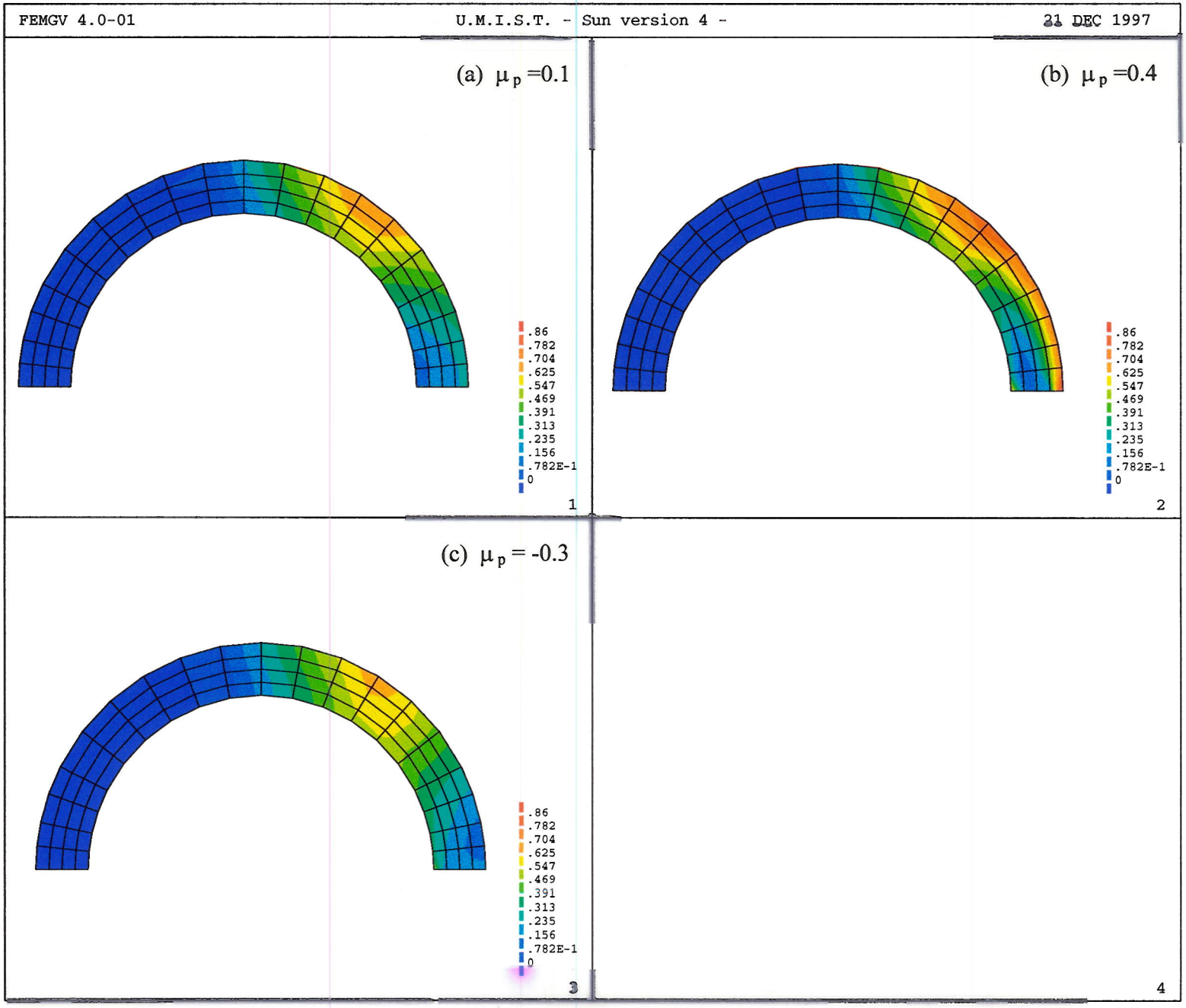


Figure 6.12 Normalized shear stresses on the interface with soft packing and $\beta=0.27^0$

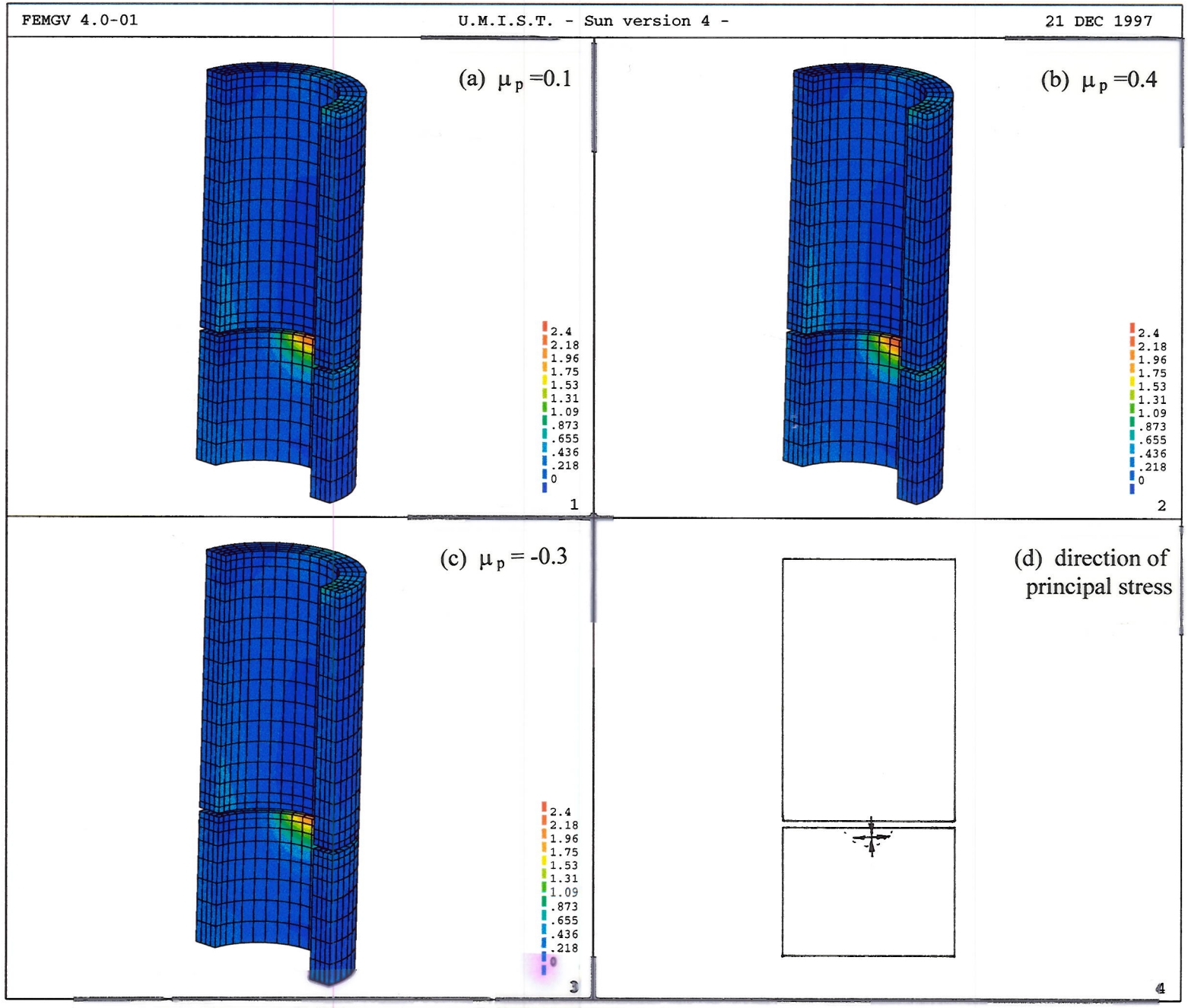


Figure 6.13 Normalized most tensile principal stresses in the pipes with soft packing and $\beta=0.27^0$

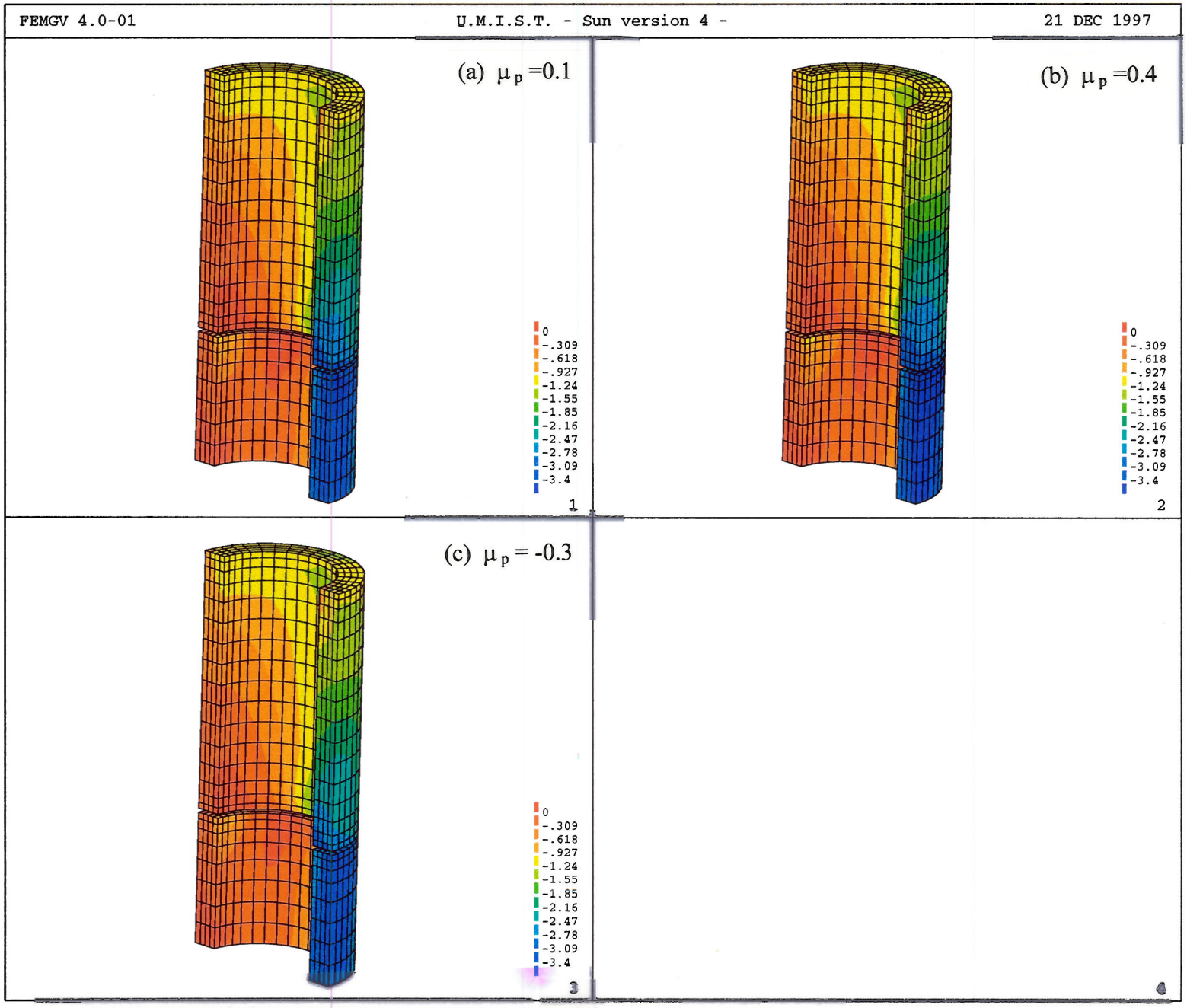


Figure 6.14 Normalized most compressive principal stresses in the pipes with soft packing and $\beta=0.27^0$

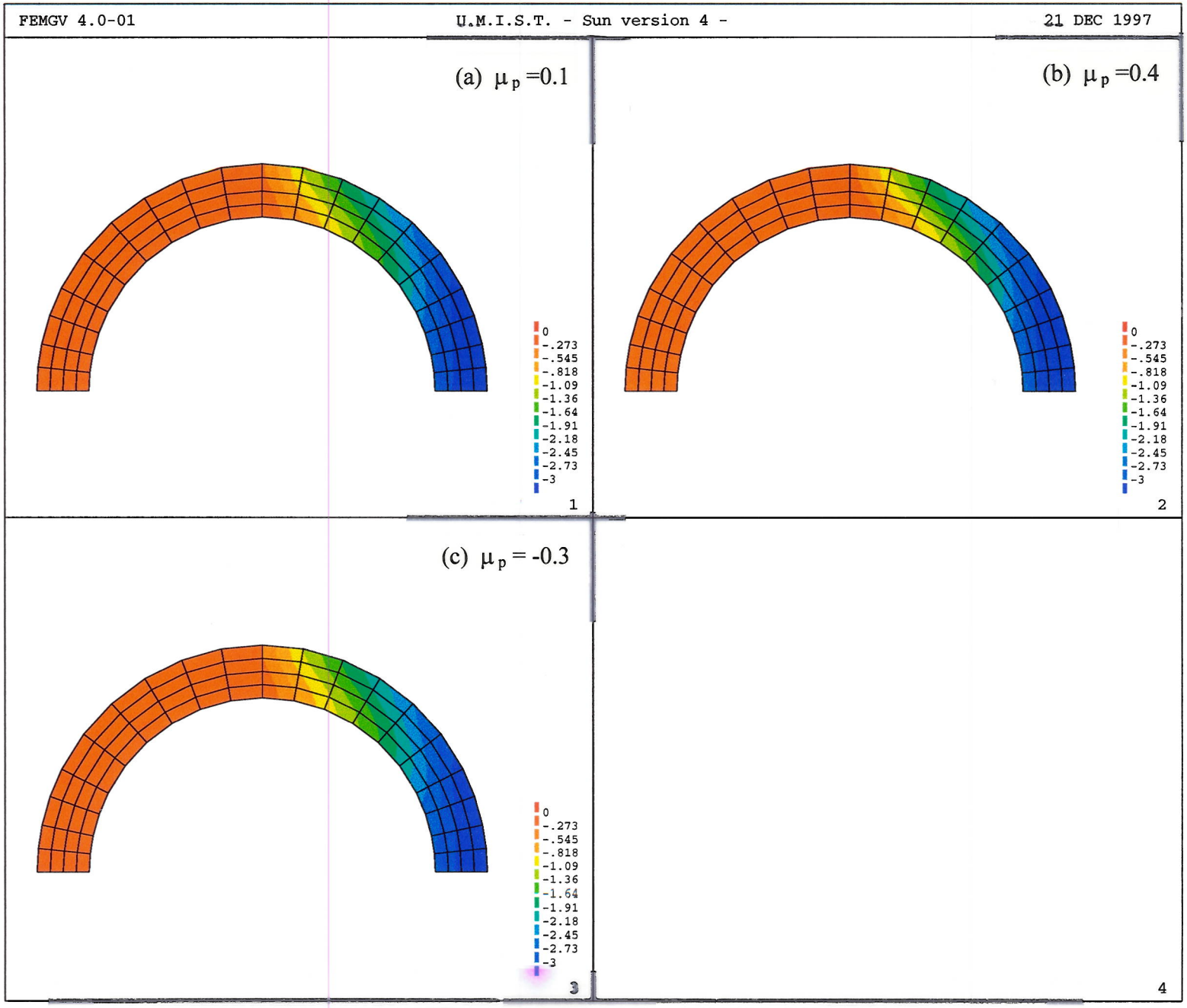


Figure 6.15 Normalized normal stresses on the interface with stiff packing and $\beta=0.27^0$

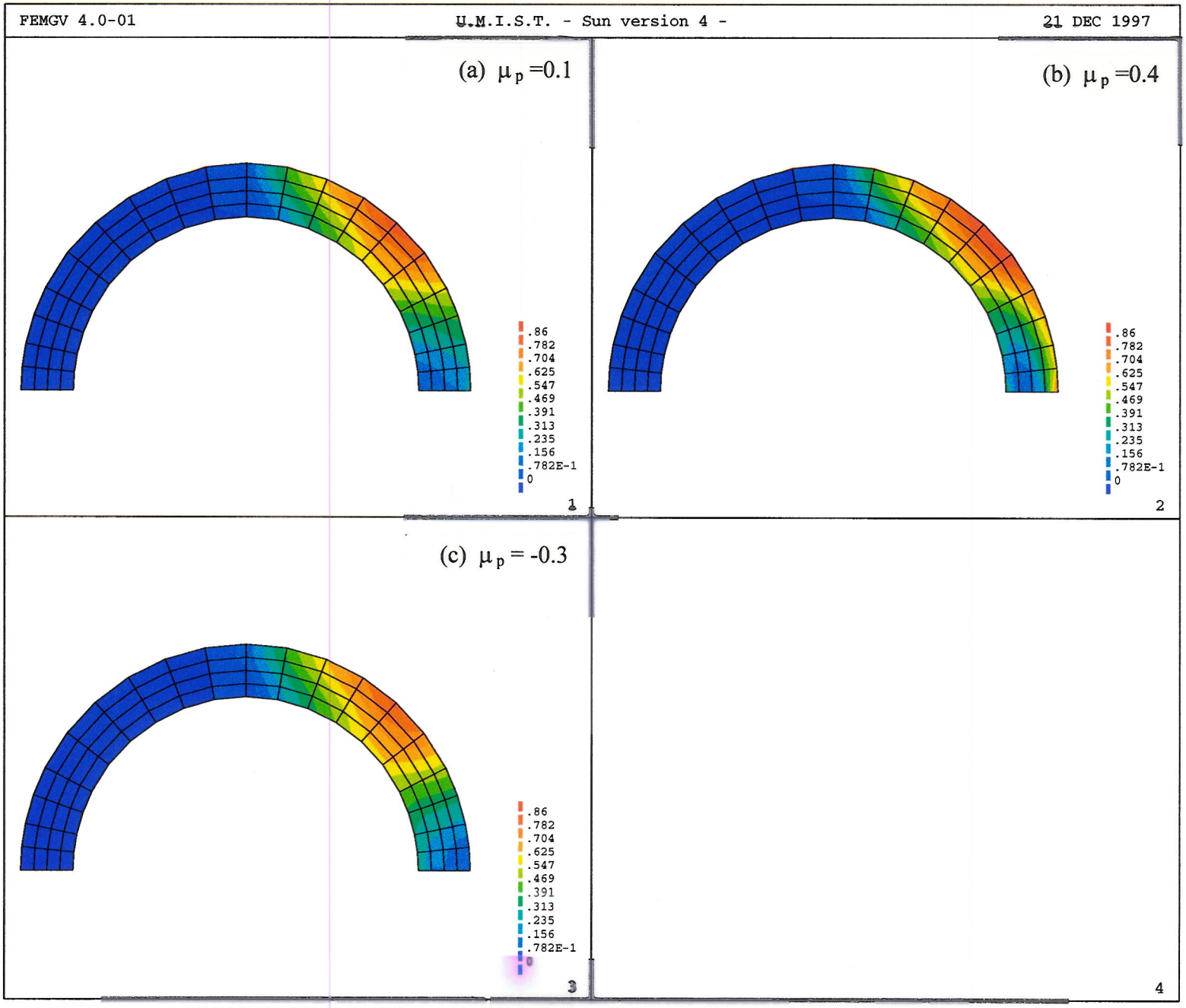


Figure 6.16 Normalized shear stresses on the interface with stiff packing and $\beta=0.27^0$

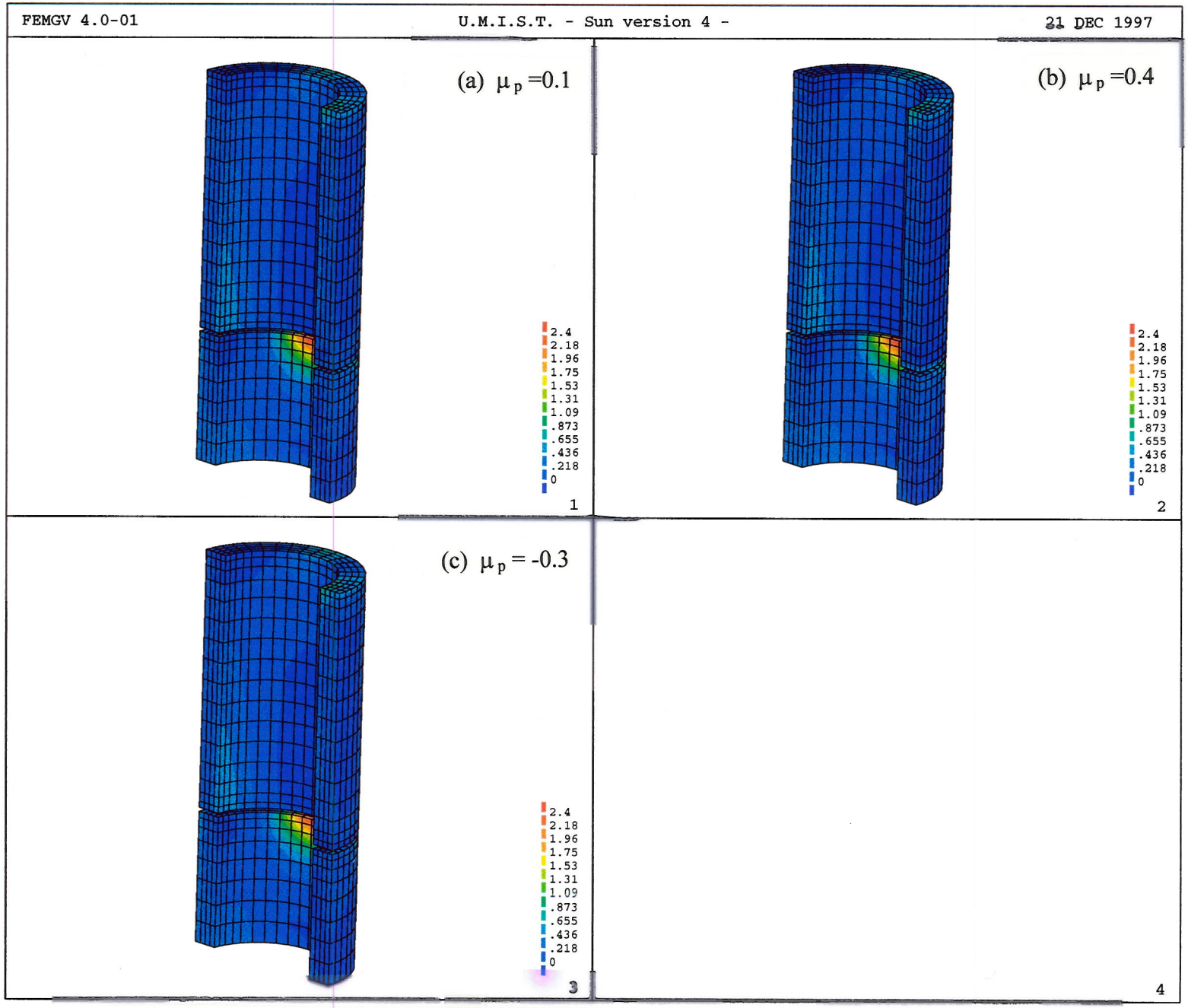


Figure 6.17 Normalized most tensile principal stresses in the pipes with stiff packing and $\beta=0.27^0$